

# Thermometric quantum sensor using excited state of silicon vacancy centers in 4H-SiC devices



Cite as: Appl. Phys. Lett. **118**, 044001 (2021); <https://doi.org/10.1063/5.0027603>

Submitted: 30 August 2020 . Accepted: 04 December 2020 . Published Online: 25 January 2021

 Tuan Minh Hoang,  Hitoshi Ishiwata, Yuta Masuyama,  Yuichi Yamazaki,  Kazutoshi Kojima, Sang-Yun Lee,  Takeshi Ohshima,  Takayuki Iwasaki, Digh Hisamoto, and  Mutsuko Hatano

## COLLECTIONS

Paper published as part of the special topic on [Hybrid Quantum Devices HQD2021](#)

 This paper was selected as Featured

 This paper was selected as Scilight



View Online



Export Citation



CrossMark

## ARTICLES YOU MAY BE INTERESTED IN

[Quantum sensor monitors the temperature inside a silicon carbide device](#)

Scilight **2021**, 051101 (2021); <https://doi.org/10.1063/10.0003408>

[Simultaneous thermometry and magnetometry using a fiber-coupled quantum diamond sensor](#)

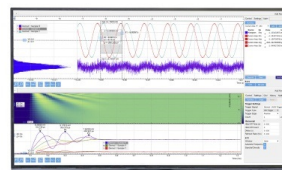
Applied Physics Letters **118**, 034001 (2021); <https://doi.org/10.1063/5.0031502>

[Carrier dynamics of silicon vacancies of SiC under simultaneous optically and electrically excitations](#)

Applied Physics Letters **118**, 021106 (2021); <https://doi.org/10.1063/5.0028318>

Challenge us.

What are your needs for periodic signal detection?



Zurich Instruments



# Thermometric quantum sensor using excited state of silicon vacancy centers in 4H-SiC devices



Cite as: Appl. Phys. Lett. **118**, 044001 (2021); doi: [10.1063/5.0027603](https://doi.org/10.1063/5.0027603)

Submitted: 30 August 2020 · Accepted: 4 December 2020 ·

Published Online: 25 January 2021



View Online



Export Citation



CrossMark

Tuan Minh Hoang,<sup>1</sup> Hitoshi Ishiwata,<sup>1,2</sup> Yuta Masuyama,<sup>3</sup> Yuichi Yamazaki,<sup>3</sup> Kazutoshi Kojima,<sup>4</sup> Sang-Yun Lee,<sup>5</sup> Takeshi Ohshima,<sup>3</sup> Takayuki Iwasaki,<sup>1,2</sup> Digh Hisamoto,<sup>1,6</sup> and Mutsuko Hatano<sup>1,3,a)</sup>

## AFFILIATIONS

<sup>1</sup>Department of Electrical and Electronic Engineering, Tokyo Institute of Technology, Meguro, Tokyo 152-8552, Japan

<sup>2</sup>PRESTO, Japan Science and Technology Agency, Chiyoda, Tokyo 102-0076, Japan

<sup>3</sup>National Institutes for Quantum and Radiological Science and Technology, Takasaki, Gunma 370-1292, Japan

<sup>4</sup>National Institute of Advanced Industrial Science and Technology, Tsukuba, Ibaraki 305-8568, Japan

<sup>5</sup>Department of Physics and Photon Science at Gwangju Institute of Science and Technology, Gwangju 123, South Korea

<sup>6</sup>Research and Development Group, Hitachi Ltd., Kokubunji, Tokyo 185-8601, Japan

Note: This paper is part of the Special Issue on Hybrid Quantum Devices.

<sup>a)</sup> Author to whom correspondence should be addressed: [hatano.m.ab@m.titech.ac.jp](mailto:hatano.m.ab@m.titech.ac.jp)

## ABSTRACT

We characterized the excited state (ES) and the ground state (GS) of negatively charged silicon vacancy ( $V_{\text{Si}}^-$ ) centers in hexagonal silicon carbide (4H-SiC) using optically detected magnetic resonance (ODMR) to realize thermometric quantum sensors. We report the observation of inverted contrast between ODMR signals of the ES and the GS and clarify the effect of energy sublevels of spin states in 4H-SiC. We confirm that ES ODMR signals of  $V_{\text{Si}}^-$  centers are dependent on the temperature with a thermal shift of 2 MHz/K on zero-field splitting (ZFS). Thus, we fabricated microscale dots of  $V_{\text{Si}}^-$  centers in a 4H-SiC p-n diode using proton beam writing and demonstrated the operation of thermometric quantum sensors by measuring the temperature change induced by an injected current. Our demonstration paves the way for the development of atomic-size thermometers inside SiC power devices for future applications.

Published under license by AIP Publishing. <https://doi.org/10.1063/5.0027603>

Silicon carbide (SiC) is one of the most promising materials for high-power and high-temperature electronic devices owning properties such as high thermal conductivity and high breakdown field.<sup>1,2</sup> In recent years, SiC has emerged as an ideal solid-state host of color centers, which act as efficient single photon emitters and are desirable for quantum applications.<sup>3,4</sup> Similar to well-studied nitrogen vacancy ( $NV^-$ ) centers in diamond,<sup>5,6</sup> negatively charged silicon vacancy ( $V_{\text{Si}}^-$ ) centers in 4H-SiC are sensitive to the magnetic field,<sup>7,8</sup> electric field,<sup>9</sup> and temperature.<sup>10,11</sup> This implies that  $V_{\text{Si}}^-$  centers can be used as a quantum thermometric sensor to directly monitor the temperature variation of SiC devices, which is required for the improvement of the performance and reliability of these devices. To date, only a few studies<sup>10,11</sup> have discussed the temperature sensing aspect of  $V_{\text{Si}}^-$  centers and the underlying physics is yet to be understood.

In this study, we showed the properties of the optically detected magnetic resonance (ODMR) signals of the ground state (GS) and the excited state (ES) of  $V_{\text{Si}}^-$  centers in 4H-SiC. Then, we demonstrated thermometric quantum sensors that can be used to measure

temperatures inside the operating SiC devices. We formed a spatially local pattern of  $V_{\text{Si}}^-$  centers in a SiC device (p-n diode) using proton beam writing (PBW)<sup>12-14</sup> and measured the temperature change resulting from the forward current injection. In our experiments, we found that the ODMR signals of  $V_{\text{Si}}^-$  centers have unique characteristics caused by the spin-orbit coupling and spin-spin interaction resulting from the crystal structure of 4H-SiC.<sup>15</sup>

$V_{\text{Si}}^-$  centers were created in a 4H-SiC bulk sample and a 4H-SiC device. For the bulk sample, the semi-insulating 4H-SiC substrate (Si-face) was irradiated with 2 MeV electron beams (EB)<sup>16</sup> with a dose of  $10^{18} \text{ cm}^{-2}$  at room temperature. During irradiation, the sample was placed on a water-cooled Cu plate to avoid heating. To remove unnecessary defects, the sample was thermally annealed at 800 °C in vacuum for 90 min. For the device, a planar SiC p-n diode was fabricated on a p-type epitaxial layer of 4H-SiC grown on an n-type 4H-SiC substrate (4° off, Si-face) by chemical vapor deposition. The aluminum acceptor concentration in the epitaxial layer was approximately  $1.45 \times 10^{16} \text{ cm}^{-3}$ . The p<sup>+</sup>-type and n<sup>+</sup>-type contact regions were created

by implanting phosphorus and aluminum at 800 °C with densities of  $5 \times 10^{19} \text{ cm}^{-3}$  and  $2 \times 10^{20} \text{ cm}^{-3}$ , respectively. Postimplantation annealing was performed at 1800 °C for 10 min. Aluminum electrodes were formed in these contact regions. We created three rows of dots of  $V_{\text{Si}}^-$  centers in the p-n junction of the diode using the PBW technique. Each dot had a diameter of 1  $\mu\text{m}$  and was generated by a 0.5 MeV proton beam at a fluence of  $3 \times 10^7 \text{ H}^+$ . We have confirmed that proton irradiation at a fluence of  $3 \times 10^7 \text{ H}^+$  does not affect the electrical characteristics of SiC pn diodes.<sup>14</sup> All the dots were separated by a distance of 10  $\mu\text{m}$ . Finally, the device was thermally annealed at 400 °C in vacuum for 30 min to remove unnecessary defects. Details of the device fabrication process and the creation of  $V_{\text{Si}}^-$  centers using PBW are described in Ref. 14.

We recorded the photoluminescence spectrum of the bulk 4H-SiC sample at room temperature using a home-built confocal microscope. In the spectrum, we observed maximum intensity at approximately 900 nm corresponding to the signatures of  $V_{\text{Si}}^-$  centers in 4H-SiC.<sup>17–19</sup> ODMR measurements were performed at room temperature for sensing the magnetic field and temperature. The ODMR experimental setup is illustrated in Fig. 1. Continuous wave (CW) lasers with wavelengths of 532 and 671 nm were used for optical pumping to confirm the effects of the excitation energy on the ODMR signals of  $V_{\text{Si}}^-$  centers. The transitions between the spin sublevels of the GS and ES were controlled by the application of radio frequency (RF) signals through a 30  $\mu\text{m}$  diameter copper wire spanned across the sample.

As shown in Fig. 2, we observed the ODMR signal of  $V_{\text{Si}}^-$  centers in the bulk 4H-SiC sample with a wide range of RF frequencies ranging from 50 MHz to 1 GHz. The ODMR spectrum has a peak with positive contrast at a resonance frequency of 70 MHz corresponding to the zero-field splitting (ZFS) of  $V_{\text{Si}}^-$  centers in the GS,<sup>13,20,21</sup> whereas a dip with negative contrast was observed at a higher resonance frequency of 440 MHz, plausibly corresponding to the ZFS of  $V_{\text{Si}}^-$  centers in the ES.<sup>10</sup> The observed result is anomalous because the spin conserving optical pumping between the GS and the ES usually leads to the same peak or dip shape of the GS and ES ODMR signals. The mechanism of this behavior will be discussed based on the energy

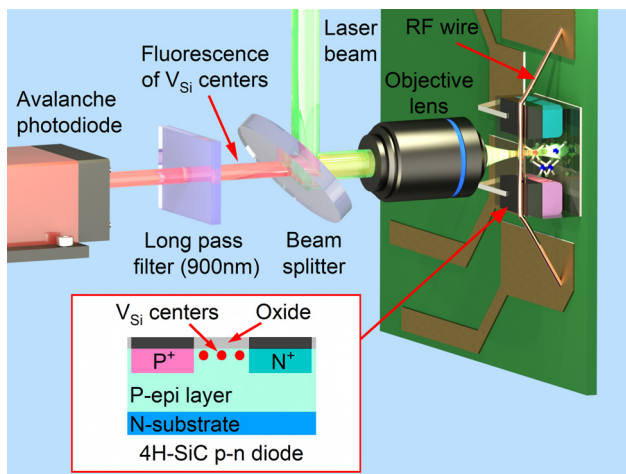


FIG. 1. Simple diagram of the ODMR experimental setup.

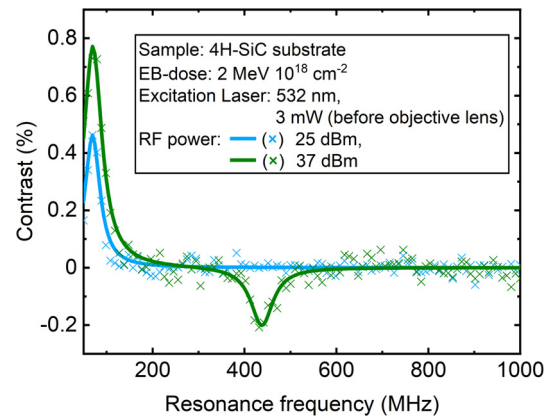


FIG. 2. GS and ES ODMR spectra of  $V_{\text{Si}}^-$  centers in the 4H-SiC bulk sample in the absence of an external magnetic field. The blue and green solid curves represent the Lorentzian fitting of the spectrum at RF powers of 25 dBm and 37 dBm, respectively.

levels of spin states later in this report. In addition, under lower RF powers (below 25 dBm), the ODMR dip cannot be observed due to the limited lifetime in the ES of  $V_{\text{Si}}^-$  centers, as shown in Fig. 2. Therefore, in this study, we used the RF powers of 20 and 37 dBm for ODMR experiments in the GS and the ES, respectively.

Now, we discuss the magnetic field-dependent properties of  $V_{\text{Si}}^-$  centers in the GS and the ES. When a magnetic field is applied parallel to the c-axis of the 4H-SiC crystal, two spin sublevels of the GS are further split into four sublevels due to the Zeeman effect.<sup>22</sup> Thus, we can observe the splitting of an ODMR peak into two peaks, and these peaks shift linearly as the magnetic field strength increases.<sup>23</sup> Figure 3 shows the obtained GS ODMR signals of  $V_{\text{Si}}^-$  centers in different magnetic fields. In zero field, we observed an ODMR peak at the resonance frequency of 70 MHz, consistent with the results shown in Fig. 2. This peak is further split into two peaks when an external magnetic field is applied parallel to the c-axis of the 4H-SiC crystal. These two peaks shift linearly depending on the magnetic field strengths of 1.1 mT and

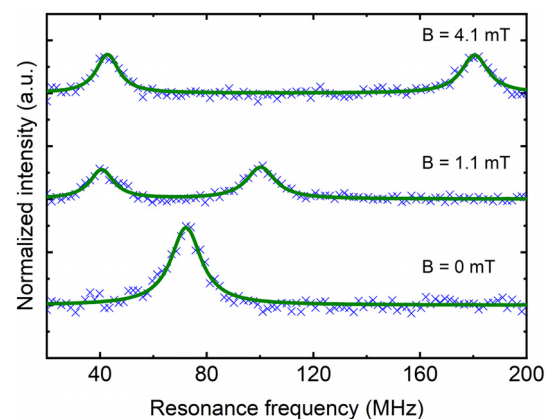


FIG. 3. GS ODMR spectra of  $V_{\text{Si}}^-$  centers in the 4H-SiC bulk sample using 532 nm excitation at magnetic field strengths of 0, 1.1, and 4.1 mT. The data were fitted using a Lorentzian function.

4.1 mT. The obtained results are consistent with demonstrations of the GS ODMR signals of  $V_{\text{Si}}^-$  centers reported in a previous work.<sup>11</sup>

Next, the magnetic field dependence of the ES ODMR signals of  $V_{\text{Si}}^-$  centers was measured with two different excitation lasers, as shown in Fig. 4(a). The ES ODMR signals measured with excitation wavelengths of 532 and 671 nm are shown in green and red, respectively. The excitation laser powers in the two cases are different due to limitations of experimental equipment. In particular, the laser powers before the objective lens are 3 and 0.1 mW for excitation wavelengths of 532 and 671 nm, respectively. In zero field, both signals show a dip shape at the resonance frequency of approximately 440 MHz, which is nearly the same as the ES ZFS of  $V_{\text{Si}}^-$  centers in a previous report.<sup>10</sup> By applying a magnetic field, the dip of each ES ODMR signal splits into two dips, and these dips shift linearly depending on the strengths of the magnetic field. The magnetic field-dependent splitting of these ES ODMR signals is in agreement with the previous work.<sup>10</sup> We should also mention that the shape of the ES ODMR signals is not dependent on the excitation wavelength.

Here, we discuss the shape of the GS and ES ODMR signals using the theoretical model proposed by Soykal *et al.*<sup>15</sup> According to this model, the energy level of the spin sublevel of  $m_s = \pm 3/2$  is lower than that of  $m_s = \pm 1/2$  in the GS due to the spin-orbit coupling and spin-spin interaction. However, this order inverts in the ES, as illustrated in Fig. 4(b). In addition, this model suggests that the fluorescence intensity is higher when  $m_s = \pm 1/2$  is populated because  $m_s = \pm 3/2$  has a faster nonradiative transition via the metastable state (MS). Thus, when we apply the RF (e.g., 70 MHz at  $B = 0$  mT) corresponding to the GS ZFS of  $V_{\text{Si}}^-$  centers, the population of the spin sublevel of  $m_s = \pm 1/2$  in the GS increases, while that of  $m_s = \pm 3/2$  decreases, as illustrated in Fig. 4(c). By optical pumping, the population of the spin sublevel of  $m_s = \pm 1/2$  in the ES becomes higher than that of  $m_s = \pm 3/2$ . Subsequently, most of the electrons in the ES with  $m_s = \pm 1/2$  directly return to the GS, while electrons with  $m_s = \pm 3/2$  mainly return to the GS through the MS without emitting fluorescence. As a result, we

observe an increase in the fluorescence intensity, which results in a peak in the GS ODMR signals. In contrast, when we apply the RF (e.g., 440 MHz at  $B = 0$  mT) corresponding to the ES ZFS of  $V_{\text{Si}}^-$  centers, the population of the spin sublevel of  $m_s = \pm 3/2$  in the ES increases, while that of  $m_s = \pm 1/2$  decreases. Therefore, electrons in the ES with  $m_s = \pm 3/2$  returning to the GS through the MS increase, as illustrated in Fig. 4(d). As a result, we can observe a decrease in the fluorescence intensity, which results in a dip in the ES ODMR signals. Our experimental results are in agreement with this mechanism.

Next, we measured the temperature dependence of the ES ZFS of  $V_{\text{Si}}^-$  centers, as shown in Fig. 5. The ES ODMR dips shift toward lower resonance frequencies when the temperature is increased, as shown in Figs. 5(a) and 5(b). By plotting the positions of the ES ODMR dips as a function of temperature, we obtained a thermal shift of 2 MHz/K, as shown in the inset of Fig. 5(c). This thermal shift is consistent with the result from a previous report,<sup>24</sup> and is not dependent on the excitation wavelength.

This high temperature resolution can provide a very effective use for power devices whose thermal information is important for device reliability. To demonstrate the application of  $V_{\text{Si}}^-$  centers, we measured the local temperature of the operating SiC p-n diode. We used PBW to create microsized dots of  $V_{\text{Si}}^-$  centers in the device. We confirmed that there are no differences in the signals of  $V_{\text{Si}}^-$  centers between the bulk sample and the device sample. A confocal microscope image of the diode was obtained to confirm the formation of dots of  $V_{\text{Si}}^-$  centers, as shown in Fig. 6(a). The I-V characteristics of the diode are shown in Fig. 6(b). Typical forward characteristics of a p-n diode are observed. Thus, the current increases with increasing voltage, and at a voltage of 30 V, current flowing through the channel width of 50  $\mu\text{m}$  is 8.3 mA and the corresponding current density is 0.166 mA/ $\mu\text{m}$ . This current results in a self-heating effect in the channel, as described below.

The local temperature distribution in the channel was controlled by the current flowing through the p-n junction. Figure 6(c) shows

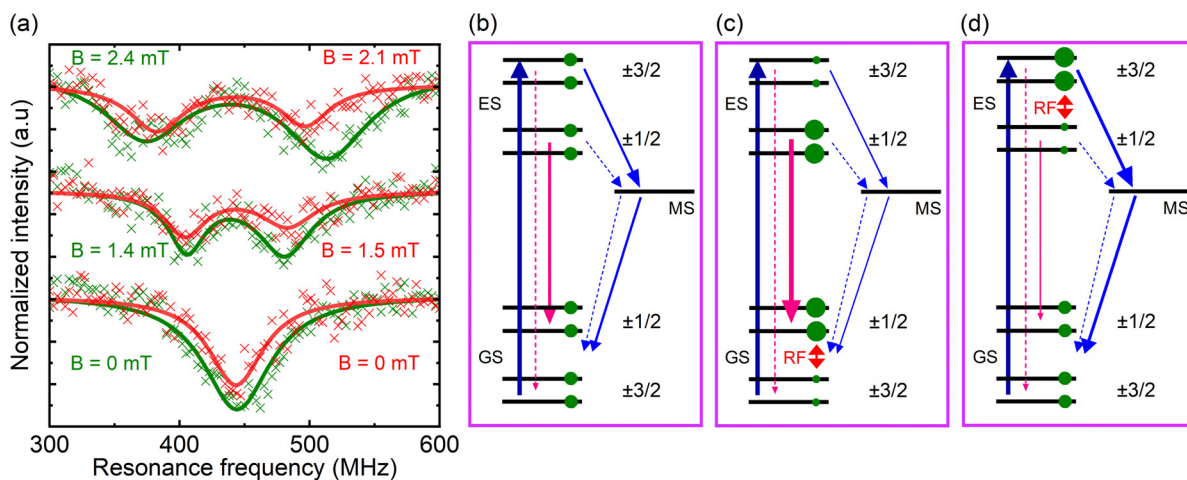


**FIG. 4.** (a) Magnetic field-dependent ES ODMR spectra of  $V_{\text{Si}}^-$  centers in the 4H-SiC bulk sample at different excitation wavelengths of 532 nm (green curves) and 671 nm (red curves). (b) Spin polarization processes of  $V_{\text{Si}}^-$  centers during off resonance. The size of green circles indicates the spin population. The population of the spin sublevel of  $m_s = \pm 3/2$  and  $m_s = \pm 1/2$  in the GS and the ES is equally polarized. (c) When the RF is applied to the GS, the spin sublevel of  $m_s = \pm 1/2$  is preferentially populated. (d) An application of the RF to the ES results in an increase in the population of the spin sublevel of  $m_s = \pm 3/2$ . The thick dashed pink and blue lines indicate a higher intensity of fluorescence and a faster rate of nonradiative decay via the metastable state (MS), respectively.

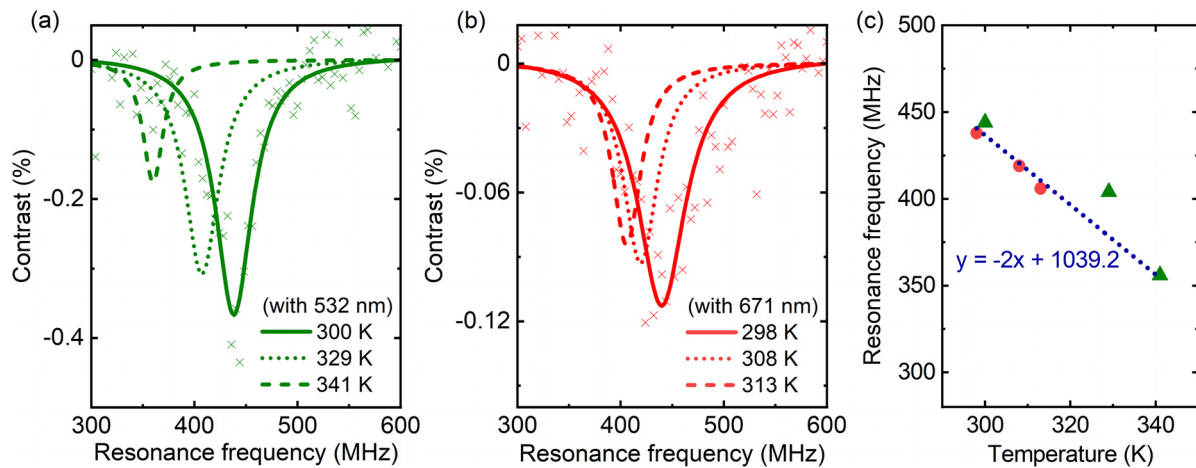


**FIG. 5.** Temperature-dependent ES ODMR spectra of  $V_{Si}^-$  centers in the 4H-SiC bulk sample at different excitation wavelengths of 532 nm (a) and 671 nm (b). The solid, dotted, and dashed lines are Lorentzian fitting curves. The data for the temperatures of 300 K and 298 K are represented. (c) Position of ES ODMR dips as a function of temperature for excitation at 531 nm (green symbols) and 671 nm (red symbols).

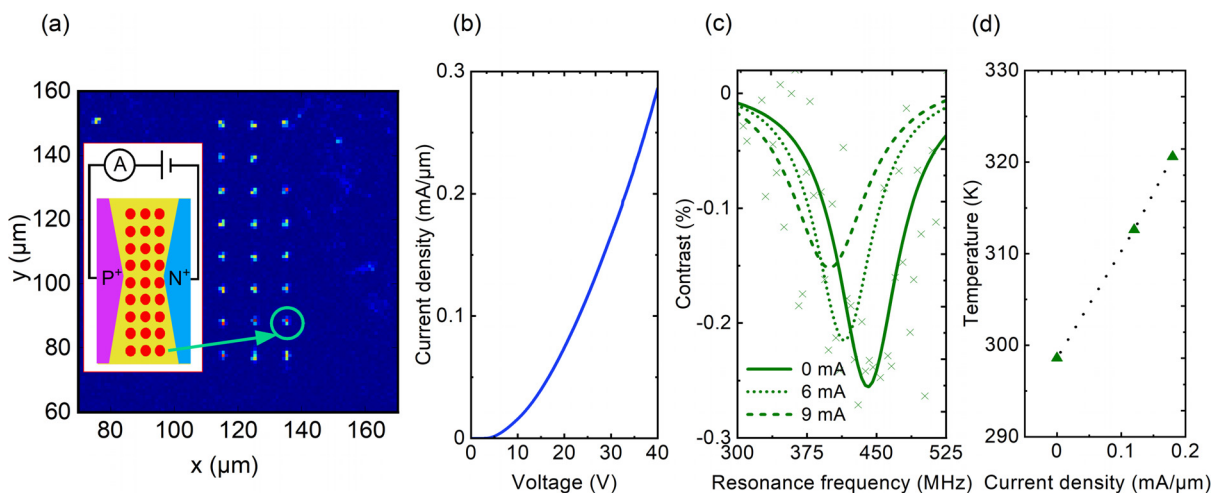


**FIG. 6.** (a) Confocal microscope image of the planar 4H-SiC p-n diode. Inset: schematic drawing of the equivalent circuit and the diode with dots of  $V_{Si}^-$  centers (red symbols) localized at the p-n junction. (b) I-V characteristic of the planar 4H-SiC p-n diode. (c) ES ODMR signals at the target position [marked with a light green circle in (a)] in the diode at different currents of 0, 6, and 9 mA. The solid, dotted, and dashed lines are Lorentzian fitting curves. The data for the current of 0 mA are shown in multiplication signs. (d) Local temperature of the target position as a function of current.

the ES ODMR signals of  $V_{Si}^-$  centers that were measured at the marked position [light green circle in Fig. 6(a)]. At 0 mA, we observed the ES ODMR dip at the resonance frequency of 440 MHz. When the current was increased, this dip shifted to lower resonance frequencies. Based on the relationship between the temperature and positions of the ES ODMR dips obtained from Fig. 5, we monitored the temperature values of 299, 313, and 321 K at the marked position, corresponding to currents of 0, 6, and 9 mA, respectively, as shown in Fig. 6(d). The temperature linearly increases with increasing current. This result indicates that quantum sensing with  $V_{Si}^-$  centers can give us the thermal information of local areas in SiC devices under operation.

In conclusion, we investigated the properties of  $V_{Si}^-$  centers in 4H-SiC as a function of the magnetic field and temperature using

ODMR. We reported an inverted contrast between the GS and ES ODMR signals and explained it based on the theoretical mechanism of the energy levels of the spin states. We confirmed that the ES ZFS of  $V_{Si}^-$  centers depends on the temperature with a thermal shift of 2 MHz/K in the bulk 4H-SiC sample. Finally, the ES ZFS of the  $V_{Si}^-$  centers was measured inside the 4H-SiC p-n diode to observe the temperature change induced by the injected current. The demonstration of monitoring the local temperature in the diode indicates that  $V_{Si}^-$  centers can be utilized as atomic-sized sensors for thermal imaging of SiC power devices.

The authors would like to thank Professor Y. Matsushita of Tokyo Institute of Technology and Dr. G. Astakhov of the Institute

of Ion Beam Physics and Materials Research HZDR for helpful discussions. This work was partially supported by the MEXT Quantum Leap Flagship Program (Grant No. JPMXS0118067395) and JSPS KAKENHI (Nos. 17H01056, 18H03770, and 20H00355). This study was carried out within the framework of IAEA CRP No. F11020. S.-Y.L. acknowledges the GIST Research Institute (GRI) grant and the Global University Project (GUP) grant funded by the GIST in 2020.

#### DATA AVAILABILITY

The data that support the findings of this study are available from the corresponding author upon reasonable request.

#### REFERENCES

- <sup>1</sup>H. Matsunami, *Microelectron. Eng.* **83**, 2 (2006).
- <sup>2</sup>A. Hefner, S.-H. Ryu, B. Hull, D. Berning, C. Hood, J. M. Ortiz-Rodriguez, A. Rivera-Lopez, T. Duong, A. Akuffo, and M. Hernandez-Mora, *Conference Record of the 2006 IEEE Industry Applications Conference Forty-First IAS Annual Meeting* (IEEE, 2006), p. 330.
- <sup>3</sup>P. G. Baranov, A. P. Bundakova, A. A. Soltamova, S. B. Orlinskii, I. V. Borovykh, R. Zondervan, R. Verberk, and J. Schmidt, *Phys. Rev. B* **83**, 125203 (2011).
- <sup>4</sup>S. Castelletto and A. Boretti, *J. Phys.* **2**, 022001 (2020).
- <sup>5</sup>C. Schreyvogel, V. Polyakov, R. Wunderlich, J. Meijer, and C. E. Nebel, *Sci. Rep.* **5**, 12160 (2015).
- <sup>6</sup>L. J. Rogers, S. Armstrong, M. J. Sellars, and N. B. Manson, *New J. Phys.* **10**, 103024 (2008).
- <sup>7</sup>M. Niethammer, M. Widmann, S.-Y. Lee, P. Stenberg, O. Kordina, T. Ohshima, N. T. Son, E. Janzén, and J. Wrachtrup, *Phys. Rev. Appl.* **6**, 034001 (2016).
- <sup>8</sup>S. G. Carter, Ö. O. Soykal, P. Dev, S. E. Economou, and E. R. Glaser, *Phys. Rev. B* **92**, 161202(R) (2015).
- <sup>9</sup>G. Wolfowicz, S. J. Whiteley, and D. D. Awschalom, *Proc. Natl. Acad. Sci.* **115**, 7879 (2018).
- <sup>10</sup>D. Simin, V. A. Soltamov, A. V. Poshakinskiy, A. N. Anisimov, R. A. Babunts, D. O. Tolmachev, E. N. Mokhov, M. Trupke, S. A. Tarasenko, A. Sperlich, P. G. Baranov, V. Dyakonov, and G. V. Astakhov, *Phys. Rev. X* **6**, 031014 (2016).
- <sup>11</sup>H. Kraus, V. A. Soltamov, F. Fuchs, D. Simin, A. Sperlich, P. G. Baranov, G. V. Astakhov, and V. Dyakonov, *Sci. Rep.* **4**, 5303 (2014).
- <sup>12</sup>T. Ohshima, T. Satoh, H. Kraus, G. V. Astakhov, V. Dyakonov, and P. G. Baranov, *J. Phys. D* **51**, 333002 (2018).
- <sup>13</sup>H. Kraus, D. Simin, C. Kasper, Y. Suda, S. Kawabata, W. Kada, T. Honda, Y. Hijikata, T. Ohshima, V. Dyakonov, and G. V. Astakhov, *Nano Lett.* **17**, 2865 (2017).
- <sup>14</sup>Y. Yamazaki, Y. Chiba, T. Makino, S.-I. Sato, N. Yamada, T. Satoh, Y. Hijikata, K. Kojima, S.-Y. Lee, and T. Ohshima, *J. Mater. Res.* **33**, 3355 (2018).
- <sup>15</sup>Ö. O. Soykal, P. Dev, and S. E. Economou, *Phys. Rev. B* **93**, 081207(R) (2016).
- <sup>16</sup>A. Kawasuso, M. Yoshikawa, H. Itoh, R. Krause-Rehberg, F. Redmann, T. Higuchi, and K. Betsuyaku, *Physica B* **376-377**, 350 (2006).
- <sup>17</sup>F. Fuchs, B. Stender, M. Trupke, D. Simin, J. Pflaum, V. Dyakonov, and G. V. Astakhov, *Nat. Commun.* **6**, 7578 (2015).
- <sup>18</sup>J.-F. Wang, Q. Li, F.-F. Yan, H. Liu, G.-P. Guo, W.-P. Zhang, X. Zhou, L.-P. Guo, Z.-H. Lin, J.-M. Cui, X.-Y. Xu, J.-S. Xu, C.-F. Li, and G.-C. Guo, *ACS Photonics* **6**, 1736 (2019).
- <sup>19</sup>M. E. Bathen, A. Galeckas, J. Müting, H. M. Ayedh, U. Grossner, J. Coutinho, Y. K. Frodason, and L. Vines, *npj Quantum Inf.* **5**, 111 (2019).
- <sup>20</sup>D. Simin, H. Kraus, A. Sperlich, T. Ohshima, G. V. Astakhov, and V. Dyakonov, *Phys. Rev. B* **95**, 161201 (2017).
- <sup>21</sup>M. Radulaski, M. Widmann, M. Niethammer, J. L. Zhang, S.-Y. Lee, T. Rendler, K. G. Lagoudakis, N. T. Son, E. Janzén, T. Ohshima, J. Wrachtrup, and J. Vučković, *Nano Lett.* **17**, 1782 (2017).
- <sup>22</sup>D. Simin, F. Fuchs, H. Kraus, A. Sperlich, P. G. Baranov, G. V. Astakhov, and V. Dyakonov, *Phys. Rev. Appl.* **4**, 014009 (2015).
- <sup>23</sup>M. Widmann, S.-Y. Lee, T. Rendler, N. T. Son, H. Fedder, S. Paik, L.-P. Yang, N. Zhao, S. Yang, I. Booker, A. Denisenko, M. Jamali, S. A. Momenzadeh, I. Gerhardt, T. Ohshima, A. Gali, E. Janzén, and J. Wrachtrup, *Nat. Mater.* **14**, 164 (2015).
- <sup>24</sup>A. N. Anisimov, D. Simin, V. A. Soltamov, S. P. Lebedev, P. G. Baranov, G. V. Astakhov, and V. Dyakonov, *Sci. Rep.* **6**, 33301 (2016).